

Practical aspects of the quantification of sp^2 -hybridized carbon atoms in diamond-like carbon by electron energy loss spectroscopy



Xinyi Zhang^{*}, Reinhard Schneider, Erich Müller, Dagmar Gerthsen^{**}

Laboratory for Electron Microscopy, Karlsruhe Institute of Technology (KIT), Engesserstr. 7, D-76131 Karlsruhe, Germany

ARTICLE INFO

Article history:

Received 19 September 2015

Received in revised form

7 January 2016

Accepted 5 February 2016

Available online 8 February 2016

ABSTRACT

The energy loss near edge structure of the carbon-K ionization edge in electron energy loss spectra (EELS) combined with (scanning) transmission electron microscopy is used to determine the content of sp^2 -hybridized carbon atoms in diamond-like carbon (DLC) films using highly ordered pyrolytic graphite as a reference material. EELS experiments are performed under magic angle conditions to eliminate orientation-dependent intensity contributions to the C–K edge of graphite. The classical two-window method is applied with the optimized settings of energy-loss integration windows for the π^* and σ^* states. Optimization is achieved by varying the width of integration windows taking solid state physics aspects into account. Electron-transparent specimens were prepared by the focused-ion-beam technique. It is shown that damage to the specimen is induced despite application of low-energy Ga^+ -ions during the final preparation stage which leads to an error in the quantification of sp^2 -content. A model for the correction of this damage is proposed which is validated by tests on highly ordered pyrolytic graphite and the DLC materials.

© 2016 Elsevier Ltd. All rights reserved.

1. Introduction

Along with the broadening of applications of diamond-like carbon (DLC) films, studies on such materials have become increasingly interesting in the recent past. Particularly relevant is the correlation of the ratio of sp^2 - and sp^3 -hybridized C-atoms in DLC with the mechanical, thermal, optical or electrical properties [1–3]. Several techniques are suited for the determination of the ratio of sp^2 - and sp^3 -hybridized C-atoms like, e.g., X-ray photon spectroscopy [4], Raman spectroscopy [5], near edge X-ray absorption spectroscopy [6] and electron energy loss spectroscopy (EELS) [7–10]. More specifically, energy loss near edge structure (ELNES) studies in combination with (scanning) transmission electron microscopy ((S)TEM), is at present the most powerful technique to quantify the ratio of sp^2 - and sp^3 -hybridized C-atoms at high spatial resolution. The quantification is based on the ELNES of the C–K ionization edge which shows characteristic features depending on the hybridization of the C-atoms. C-atoms with sp^2 -hybridization form three planar σ bonds with an angle of 120° in

between which result from the hybridization of the $2s$ orbital with the $2p_x$ and $2p_y$ orbitals. A π bond perpendicular to the plane of the σ bonds is generated by the $2p_z$ orbital. Four σ bonds with an angle of 109° in between occur for C-atoms with sp^3 -bonding by the hybridization of the $2s$ orbitals with all three $2p$ orbitals in equal proportion. The ELNES of C-atoms is determined by unoccupied (anti-bonding) π^* and σ^* states for the differently hybridized C-atoms.

C-atoms with sp^2 -hybridization show a characteristic pre-peak in EELS spectra of the C–K ionization edge with an onset at ~ 284 eV which is associated to the excitation of $1s$ core level electrons into π^* states. Both, sp^3 - and sp^2 -hybridized C-atoms show a strong loss signal with an onset at ~ 290 eV which is related to the excitation of $1s$ electron into σ^* states. The loss intensities related to the excitation into π^* and σ^* are denoted in the following as I_{π^*} and I_{σ^*} . The concept for the quantification of the percentage of sp^2 -hybridized C-atoms is based on the ratio of the loss intensities (denoted as I -ratio), e.g., I_{π^*}/I_{σ^*} . The intensities I_{π^*} and I_{σ^*} depend strongly on experimental parameters such as electron energy E_0 , convergence semi-angle α , and collection semi-angle β , as well as the details of the extraction of I_{π^*} and I_{σ^*} from EELS spectra (e.g. the width of the energy integration windows). To avoid artifacts, the I -ratio of the material to be characterized is compared to a reference material with known fraction of sp^2 -hybridized C-atoms on the

^{*} Corresponding author.

^{**} Corresponding author.

E-mail addresses: Xinyi859@hotmail.com (X. Zhang), Gerthsen@kit.edu (D. Gerthsen).

basis of EELS spectra taken under identical experimental conditions and using the same evaluation procedure.

Numerous approaches have been suggested and discussed on how the I -ratio can be extracted, e.g., two-window methods [9–11], functional fitting methods [12–14], and other model fitting methods [15–17]. In this work we focus on the two-window method, because it is straightforward to use especially for material scientists rather than EELS spectroscopists with access to density functional theory (DFT) data. Although shortcomings of the two-window methods were described in the literature, we will show that an optimization is possible by an appropriate choice of the energy-window settings for I_{π^*} and I_{σ^*} . This is justified on the basis of the state of literature that will be outlined in the following.

In two-window methods [9–11] I_{π^*} and I_{σ^*} are obtained by integrating the intensity of the C–K edge over energy windows which are specific for π^* and σ^* states. Two different approaches were proposed to quantify the fraction of sp^2 -hybridized C-atoms. In both cases, I_{π^*} covers a narrow energy-loss interval associated with the π^* pre-peak. Berger et al. [10] suggested an I -ratio given by $I_{\pi^*}/I_{\Delta E}$ where $I_{\Delta E}$ starts at the onset of the π^* peak and contains I_{σ^*} up to a maximum loss energy. $I_{\Delta E}$ accounts for the sum of sp^2 - and sp^3 -hybridized C-atoms. For a C-material with an atomic fraction x of sp^2 -hybridized C-atoms, the intensity ratio $I_{\pi^*}/I_{\Delta E} = k'x/4$ is proportional to x with a proportionality factor k' . It has been already pointed out by Bruley et al. [9] that errors can occur because x depends strongly on the width of I_{π^*} and $I_{\Delta E}$ and contributions not related to π^* and σ^* states occur between the π^* pre-peak and the onset of the σ^* states. For example, the σ^* states of C–H bonds in hydrogenated C-material has been considered to cause energy losses between the π^* and σ^* states [6,8,13,18,19]. It was also reported that signals in this range could be related to non-ideal sp^2 -configuration with distorted bonding angles [14]. Moreover, C-atoms with dangling bonds can also cause excitations closely below the π^* states [20,21].

To take contributions between π^* and σ^* states into account, function fitting methods were proposed [12–14] where Gaussian or Lorentzian functions are used to model the experimental C–K edge spectrum. Shortcomings of the function fitting methods were already addressed by Bernier et al. [12] and Titantah et al. [17] because the physical justification of the number and positioning of the fit function is not straightforward. Function fitting techniques, especially those without constraints, provide a large number of fit parameters which yield fits with the same χ^2 quality for different fit parameters and, hence, ambiguous results for the fraction of sp^2 -hybridized C-atoms.

Alternatively, an I -ratio given by I_{π^*}/I_{σ^*} can be used where I_{σ^*} covers an energy window beyond the onset of the σ^* peak [10]. This I -ratio is considered to be proportional to the ratio between the number of π^* and σ^* bonds, with a proportionality factor k depending on the experimental settings and the way of determination of the I -ratio. For a graphite reference specimen pure in sp^2 -C and an unknown C-material containing a fraction x of sp^2 -hybridized C-atoms the I -ratios for the reference and unknown material can be written as

$$\left(\frac{I_{\pi^*}}{I_{\sigma^*}}\right)_{reference} = k \cdot \frac{1}{3} \quad (1)$$

$$\left(\frac{I_{\pi^*}}{I_{\sigma^*}}\right)_{unknown} = k \cdot \frac{x}{4(1-x) + 3x} = k \cdot \frac{x}{4-x} \quad (2)$$

Equation (1) can be used to remove the dependence on k in Equation (2), and thus x in the unknown C-material can be expressed as

$$x = \frac{4 \left(\frac{I_{\pi^*}}{I_{\sigma^*}}\right)_{unknown} / \left(\frac{I_{\pi^*}}{I_{\sigma^*}}\right)_{reference}}{3 + \left(\frac{I_{\pi^*}}{I_{\sigma^*}}\right)_{unknown} / \left(\frac{I_{\pi^*}}{I_{\sigma^*}}\right)_{reference}} \quad (3)$$

Using appropriate settings for the integration windows of I_{π^*} and I_{σ^*} , this I -ratio avoids some of the problems associated with the I -ratio suggested by Berger et al. [10] which are related to C–H bonds and dangling bonds of C-atoms.

Two-window methods are generally criticized because they rely on the assumption that π^* and σ^* states can be completely separated and do not overlap. Model fitting approaches [15–17] have revealed deep insights into the distribution of π^* and σ^* states in graphite and amorphous carbon (a-C) materials because the C–K edge ELNES was calculated on the basis of density functional theory (DFT). Detailed studies have indeed shown that contributions from graphite π^* states are found at higher energy [4,22,23]. Similarly, σ^* states may contribute to energy-loss intensities as low as 288 eV due to lifetime broadening [4,17,22] or a shift to lower energy losses for sp^3 -rich C-materials [21]. Titantah et al. [17] showed that a-C materials exhibit a modified density of states (DOS) compared to graphite which is typically used as a reference material. However, even in their advanced procedure, the contributions of C–H bonds, which are often relevant in DLC materials, were not taken into account. C–H bonds on the other hand were clearly shown to modify the loss intensity between the π^* and σ^* states depending on the deposition procedure and heat treatments [8].

Despite the shortcomings related to the overlap of σ^* and π^* states, we will show in this work that the Cuomo-type two-window method (Equations (1)–(3)) can be optimized with appropriate energy window settings for I_{π^*} and I_{σ^*} . It is advantageous that this technique does not rely on elaborate DFT calculations and is readily applicable for materials scientists. To optimize the two-window approach and facilitate reliable extraction of I_{π^*} and I_{σ^*} , it is a prerequisite to gain a sufficient understanding on intensity contributions to the C–K edge. With respect to the narrow π^* peak, three broadening mechanisms have to be considered: lifetime of the core hole (Lorentzian broadening), lifetime of the excited state (Lorentzian broadening) and the experimental broadening (Gaussian broadening) [24,25]. The latter is given by the full width at half maximum (FWHM) of the zero-loss peak in the EELS spectrum and remains unchanged for identical acquisition conditions. The core hole lifetime broadening of 0.06 eV can be taken from calculated values for the C–K edge [26] and is negligible for the choice of integration window compared to the other two broadening effects. The lifetime broadening effect of the excited states is more complex. Much effort has been made to treat this effect when calculating ELNES [25,27], and it was found that the π^* components in the C–K spectra is broader for a-C samples than for crystalline graphite samples, e.g., in the work of Titantah et al. [17]. This is reasonable because the excited state lifetime depends on the long-range order of the material and decreases in an aperiodic environment [24], resulting in a stronger lifetime-broadening effect of an EELS spectral feature for amorphous materials as compared to corresponding crystalline materials. Therefore, an error can occur in the sp^2 -quantification if amorphous carbon is analyzed and crystalline graphite is used as a reference material. Due to the small width of the π^* pre-peak compared to the σ^* intensity, a small variation of the setting of the π^* window could include a large fraction of erroneous signals and thus lead to a large scatter in the evaluated content of sp^2 -hybridized atoms (denoted by $sp^2\%$ in the following), and, hence, quantification is very sensitive to this setting. The energy window setting for I_{σ^*} is less sensitive but I_{σ^*} can be affected by plural scattering or errors caused by the removal

of plural scattering in the higher energy loss region of the C–K ionization edge.

Based on the considerations addressed above, by adequate choice of integration windows for I_{π^*} and I_{σ^*} , it is possible to include or exclude signals in the spectra and study the influence of any signals, that occur due to overlapping π^* and σ^* states, the lifetime broadening effect for the π^* states, density of states connected with CH– bonds or distorted C– bonds between I_{π^*} and I_{σ^*} . We have chosen in this work an approach for integration window optimization which is derived from the work of Titantah et al. [17]. They showed that the stability, i.e., a small variation sp^2 -quantification results is a characteristic feature of adequate integration window ranges. To determine optimum energy window settings for I_{π^*} and I_{σ^*} , we have varied systematically the integration boundaries over a larger energy loss range. The integration window settings were deduced from ranges with minimum standard deviation of the quantification results. Two different DLC materials with different $sp^2\%$ were studied using highly ordered pyrolytic graphite (HOPG) as a reference material.

Several other aspects are considered in our work which have not been consistently taken into account or even neglected up to now. For the first time the effect of damaged surface layers was investigated for DLC and graphite TEM specimens which are prepared by focused-ion-beam milling. We also studied the effect of plural scattering by explicitly comparing results of the sp^2 -quantification at thin and thicker TEM specimen regions. All experiments were performed at 80 keV electron energy to exclude electron-beam damage which was shown to occur in sp^2 -rich carbon materials [28]. The EELS spectra were taken under magic angle (MA) conditions [29] to eliminate orientation-dependent intensity contributions to the C–K edge due to the anisotropic graphite structure which was used as a reference in this work.

2. Experimental procedures

Two DLC films were studied in this work, which were deposited by plasma-enhanced vapor deposition on steel substrates. The samples include a hydrogenated amorphous carbon (a-C:H) film containing a relatively high $sp^2\%$ [30], and a tetrahedral amorphous carbon (ta-C) film with a lower $sp^2\%$. HOPG of ZYA grade (Mikro-Mash™) was used as a reference material. The film thicknesses were $\sim 3 \mu\text{m}$ for the a-C:H film and $\sim 2 \mu\text{m}$ for the ta-C film. Since the $sp^2\%$ possibly depends on the depth of the film, cross-section TEM lamellae were prepared by focused-ion-beam (FIB) milling using the standard lift-out technique [31]. In this process, a thick Pt/C-protection layer ($\sim 1 \mu\text{m}$) was deposited in the FIB prior to any milling, which was largely sacrificed by the following thinning procedure. 30 keV Ga^+ -ions with an ion beam of 90 pA were used for coarse thinning. During the final stage of polishing a reduced ion-beam energy of 5 keV and 70 pA were applied to minimize specimen damage. Several windows with different thickness were thinned to electron transparency in a single lamella to facilitate EELS measurements from regions of different thicknesses. To avoid any FIB-induced damage of the HOPG reference sample, a TEM specimen was also prepared by cleavage using scotch tape as described by Geim et al. [32].

For EELS acquisition, the FEI Titan³ 80–300 microscope is equipped with a GATAN imaging energy filter (GIF) Trididem model 865 HR and a 4 mega-pixel CCD camera as detector. In all STEM/EELS experiments, the Titan microscope was operated at 80 kV in the microprobe STEM mode to avoid beam damage and contamination. EELS spectra did not change during the STEM/EELS acquisition, which is indicative of negligible influence of electron-beam irradiation on the sp^2 -content. The energy dispersion of the Trididem model 865 HR was set to 0.1 eV/channel. The duration of a single

EELS acquisition of the C–K edge was 1 s, with a typical electron dose rate of several $10 \text{ e}^-/\text{\AA}^2\text{s}$. In each case, the final C–K ELNES spectrum was obtained by summing up of ~ 100 single spectra. Low-loss spectra were obtained with a similar setup, except that the electron dose rate and acquisition time were largely reduced to prevent any beam damage of the scintillator in front of the CCD chip.

The convergence semi-angle under the chosen microprobe illumination was 2.0 mrad. Using a spectrometer acceptance semi-angle of 3.9 mrad, the orientation dependence of the HOPG C–K edge spectra could be largely suppressed. This value agrees well with the MA of ~ 4.73 mrad for 80 keV that was calculated according to Hebert et al. [29]. During EELS acquisition, the HOPG specimens were first oriented close to a zone axis (ZA) and channeling effects were avoided by tilting the specimens by $5\text{--}10^\circ$ away from it.

The relative sample thickness t/λ (t : thickness, λ : mean free path for plasmon scattering) for each C–K edge spectrum was derived from low-loss spectra by the log-ratio method [7]. Measurements were performed with an energy resolution between 0.6 eV and 0.7 eV according to the FWHM of the zero-loss peak (ZLP).

C–K edge spectra processing follows the standard procedure, i.e., background subtraction by an exponential function of the type $a \cdot e^{-b}$ with a and b as fit parameters, using a pre-edge window of 30 eV width. Effects of plural scattering were removed by Fourier-ratio deconvolution with the relevant low-loss spectra.

3. Quantification of the sp^2 -content in amorphous carbon materials

3.1. Experimental results

Fig. 1 shows high-resolution TEM images of a-C:H and ta-C with the corresponding diffractograms obtained by Fourier transformation of the images. The images show that the structure is completely amorphous without any anisotropy or recognizable sp^2 -rich clusters.

Fig. 2 shows four low-loss EELS spectra, among which spectra (1) and (2) were acquired from regions of the a-C:H specimen with t/λ of 0.47 and 0.74, respectively. Spectra (3) and (4) in Fig. 2(b) were taken from regions of the ta-C specimen at t/λ of 0.58 and 1.41. For all spectra the maximum intensities of the ZLP were normalized to 1 and only 1/10 of the total intensity of the ZLP is visible. The spectra of a-C:H (Fig. 2(a)) show characteristic energy loss intensities at ~ 6 eV, which can be assigned to π plasmons [33], while the σ plasmon peaks are both centered at ~ 23 eV. The low-loss spectra for ta-C (Fig. 2(b)) are clearly different. The π plasmon is only vaguely visible, and the σ plasmon peaks are shifted to higher energy losses at 26.8 eV and 29.4 eV, respectively. The position of the σ plasmon peak gives an indication of the sp^2 -fractions. Kulik et al. [33] observed a peak shift with increasing sp^2 -content from 33.5 eV for crystalline diamond to ~ 25 eV for sp^2 -rich evaporated a-C and also found σ plasmon energies around 30 eV for ion-beam-deposited sp^2 -poor a-C. The small plasmon energy of 23 eV for a-C:H here indicates a high sp^2 -content in this material. A lower sp^2 -content can be expected in ta-C with higher plasmon energies which seems to depend on t/λ . It will be later shown, that the shift of the σ plasmon peaks in the two ta-C spectra is related to a damage layer with higher sp^2 -content than the bulk material. The damage layer is induced by the FIB preparation of the TEM specimen and corresponding change of the average sp^2 -content depends on t/λ .

In the following we study the effect of the width and boundaries of the integration windows for I_{π^*} and I_{σ^*} and consider their effect on the evaluated $sp^2\%$. Optimum integration boundaries are derived from energy loss regions with minimum variation of the evaluated

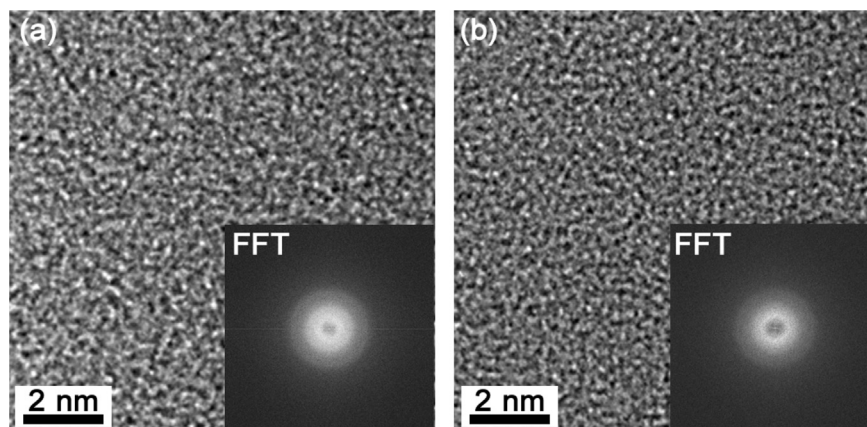


Fig. 1. High-resolution TEM images of (a) a-C:H and (b) ta-C. The inserted diffractograms show corresponding diffractograms from an imaging area four times larger than (a) and (b).

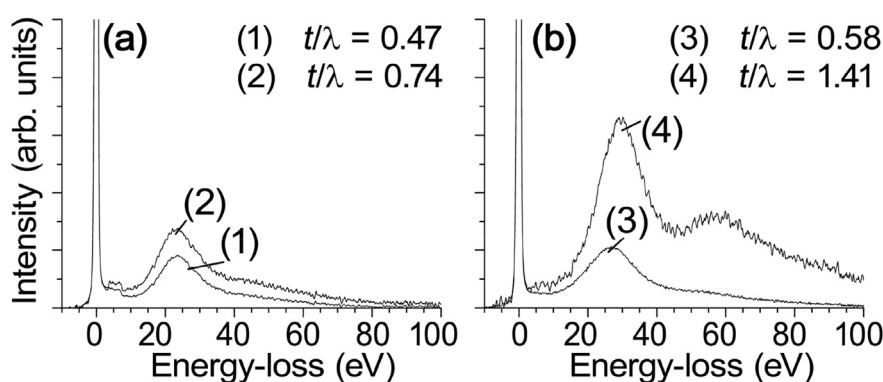


Fig. 2. Low-loss spectra acquired from (a) the a-C:H TEM specimen at a relative TEM specimen thicknesses of 0.47 (spectrum 1) and 0.74 (spectrum 2), and (b) low-loss spectra of the ta-C TEM specimen taken at relative TEM specimen thicknesses of 0.58 (spectrum 3) and 1.41 (spectrum 4).

sp^2 -content. An iterative procedure was applied by first considering the σ^* window, which is in general less sensitive for the sp^2 -quantification than the π^* window. The π^* window was set arbitrarily for the first optimization round of the σ^* window. The positions of the two boundaries of the σ^* window were tested by varying one of them separately with the other fixed to show the direct influence on the sp^2 -quantification. The π^* window was afterwards optimized by centering it at the maximum intensity of the π^* pre-peak and varying its width, using the tentatively optimized σ^* window. Both π^* and σ^* windows were iteratively optimized for a few rounds.

The last optimization round for I_{σ^*} is illustrated in Figs. 3 and 4 where the variation of the upper boundary (Fig. 3) and lower boundary (Fig. 4) of the σ^* window was optimized with a fixed π^* window between 284.7 eV and 285.3 eV (fixed boundaries indicated by the triangular symbols and drop lines in Figs. 3 and 4). ELNES quantifications are performed based on the determination of I_{π^*}/I_{σ^*} and Equation (3).

Fig. 3 shows two spectra of a-C:H (Fig. 3(a,b)) and two spectra of ta-C (Fig. 3(c,d)) as solid lines taken at different relative thicknesses. In each figure, the HOPG reference spectrum of a cleaved TEM specimen (dash-dotted line) is also included for comparison. Background and plural scattering effect are removed for all spectra. The spectra of DLCs were rescaled so that the integral intensity between 292 eV and 307 eV, which is the optimized σ^* energy window for quantification, is normalized to that of the HOPG spectrum. Already it can be seen that the spectra from a-C:H in Fig. 3(a,b) show higher π^* intensities, indicating a higher sp^2 than

ta-C. It is also noticed that the spectrum from ta-C in Fig. 3(c) with $t/\lambda = 0.58$ shows a higher π^* intensity than that in Fig. 3(d) with $t/\lambda = 1.41$, which hints at another influence of the specimen thickness on the quantified sp^2 value (apart from the plural scattering effect which has been removed) and, therefore, on a more or less pronounced effect of FIB-induced damage which will be studied in detail in Section 4.

In Fig. 3, the π^* window was set between 284.7 eV and 285.3 eV and the lower boundary of the σ^* window was fixed at 292 eV while the upper boundary was varied between 293 eV and 320 eV (35 eV above the π^* pre-peak, a small portion of plasmon intensities could be contained within this range) in 1 eV steps. Fig. 3(a,b) show the results for the a-C:H sample. The sp^2 -content, given by the dotted lines, can be subdivided into sectors I to III (cf. Fig. 3(a)). Taking the spectrum in Fig. 3(a) as an example, the quantification results show a drop of the evaluated sp^2 % for the upper σ^* boundary from 293 eV to 300 eV, followed by a stable region with little variation from 300 eV to 314 eV. Setting the upper boundary of the I_{σ^*} integration window at values between 314 eV and 320 eV, a drop of the sp^2 % can be seen again. Within each of the three sectors the standard deviations of the calculated sp^2 % are 0.046 (sector I), 0.006 (sector II), and 0.028 (sector III) for Fig. 3(a) while for Fig. 3(b) the deviations are 0.039 (sector I), 0.007 (sector II), and 0.027 (sector III). For the ta-C sample, stable quantification results are obtained in sector II with upper integration boundaries between 298 eV and 307 eV in both the thinner sample region (Fig. 3(c)) and the thicker sample region (Fig. 3(d)). Note the strongly differing sp^2 -contents in the thin and thick specimen

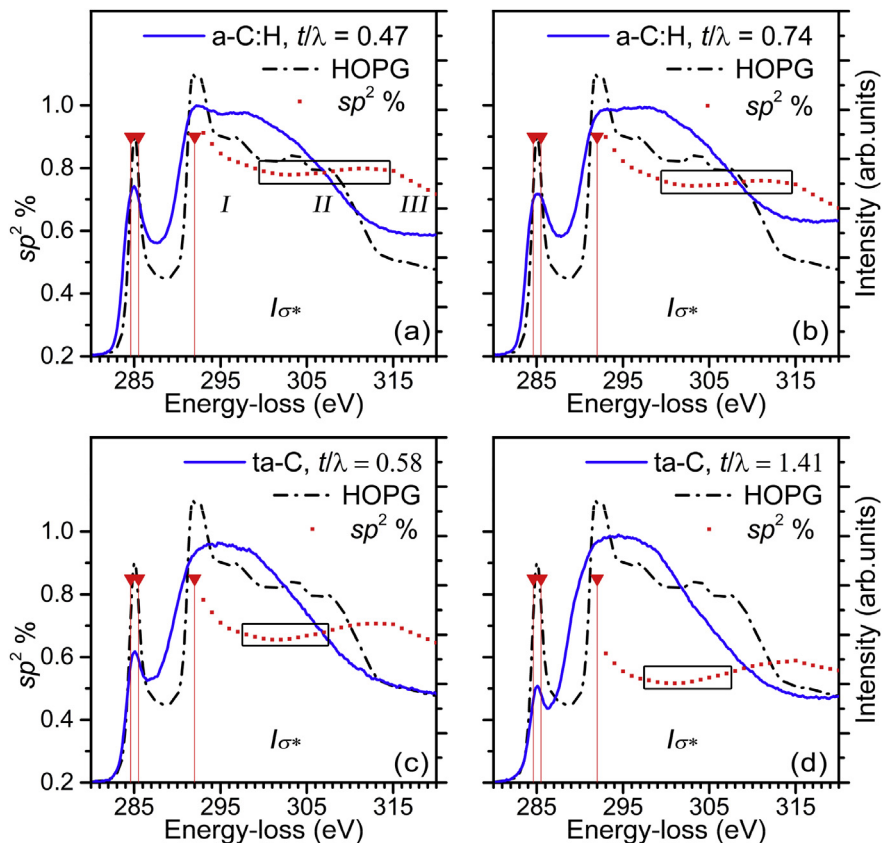


Fig. 3. ELNES quantification results (dotted lines) for the C–K edge of the (a,b) a-C:H and (c,d) ta-C from regions with different thicknesses t/λ as a function of the upper boundary of the σ^* energy window, superimposed on the corresponding sampled spectrum (solid line) and the reference HOPG spectrum (dash-dotted line). (A color version of this figure can be viewed online.)

regions of ta-C. Considering the regions with minimum variation of $sp^2\%$ in both materials, the upper integration boundary was fixed at 307 eV. This is reasonable because little dependence of the quantification results are observed up to this upper boundary.

In analogy to Fig. 3, Fig. 4 shows the effect of the lower integration boundary of I_{σ^*} between 286 eV and 306 eV on the quantified $sp^2\%$ content. The π^* window was set again between 284.7 eV and 285.3 eV and the upper boundary of the σ^* window was fixed at 307 eV. In all cases, the quantification results can also be subdivided into three sectors. Taking the spectrum in Fig. 4(a) for a-C:H as an example, first a gradual increase of $sp^2\%$ is rather clear before reaching a maximum, which is referred to as sector I. In sector II the quantification results vary only slightly but show a descending and ascending arc, with a minimum in between. The sector III shows an increase of the calculated $sp^2\%$ again, with its starting point traced back into the sector II. Sector II is slightly different for a-C:H and ta-C, namely 292–300 eV and 291–298 eV, respectively. The standard deviations of the calculated $sp^2\%$ in the three sectors for all the four spectra are (Fig. 4(a): 0.011, 0.006, 0.017) (Fig. 4(b): 0.010, 0.007, 0.018), (Fig. 4(c): 0.012, 0.006, 0.040), and (Fig. 4(d): 0.011, 0.007, 0.043). It is therefore reasonable for both materials to set the lower boundary at 292 eV and assure a σ^* window as large as possible. For the ta-C film, a large discrepancy is again observed in sector II for the thin ($sp^2\%$ of $67.6\% \pm 0.6\%$, Fig. 4(c)) and thick specimen region ($55.0\% \pm 0.7\%$, Fig. 4(d)).

After optimizing the integration window for I_{σ^*} , the same procedure was applied for I_{π^*} . The tests of the influence of width variation of the π^* window on the quantified $sp^2\%$ are based on setting the σ^* window from 292 eV to 307 eV and keeping the π^*

window centered at the maximum intensity of the π^* pre-peak (285 eV). The initial size of the π^* window (0.7 eV) was chosen slightly larger than the energy resolution (0.6 eV). Both boundaries were varied by ± 0.2 eV which yields standard deviations of the evaluated $sp^2\%$ of 0.019, 0.020, 0.015, and 0.009 for spectra in Fig. 3(a–d), also Fig. 4(a–d), yielding an optimized π^* integration window between 284.7 and 285.3 eV.

The optimized setting of integration windows for the π^* states and from 292 to 307 eV for σ^* states was applied for the quantification of overall 13 spectra from the a-C:H specimen, which yields an $sp^2\%$ of $(76.9 \pm 1.1)\%$. In more detail, for spectra acquired from regions with t/λ of 0.44–0.48, the $sp^2\%$ is $(77.2 \pm 0.7)\%$, while for spectra acquired from regions with t/λ of 0.70–0.76, the $sp^2\%$ is $(76.3 \pm 1.3)\%$. Quantification results for all 13 spectra obtained by varying again the upper boundary of the σ^* window between 300 and 314 eV, by varying the lower σ^* window boundary between 292 and 300 eV, and by varying the size of the π^* window between 0.3 and 1.1 eV (351 evaluations overall) amount to an average $sp^2\%$ of 76.6% with a standard deviation of 1.7%.

Considering for ta-C separately thin (Figs. 3(c) and 4(c)) and thicker specimen regions (Figs. 3(d) and 4(d)) yields average $sp^2\%$ -contents of $(67.2 \pm 1.2)\%$ and $(54.3 \pm 1.9)\%$ by varying the energy window setting within an optimized range. The final quantification of the $sp^2\%$ will be presented in section 4.2 because the strong dependence of the quantification results on the specimen thickness in ta-C suggests an influence of the FIB specimen preparation.

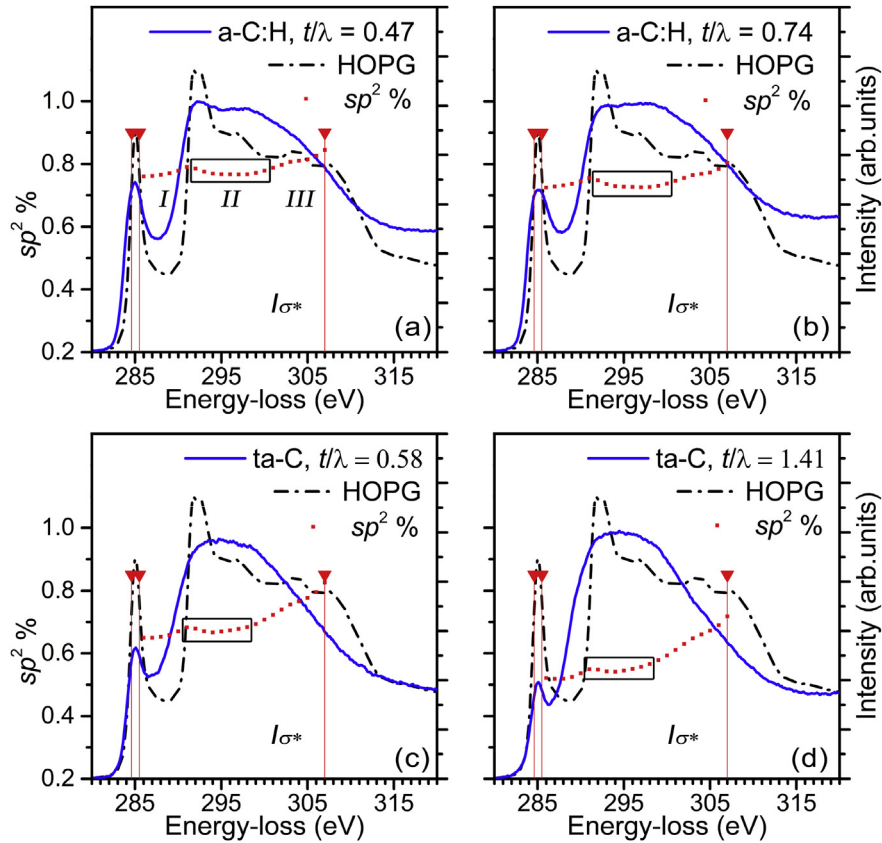


Fig. 4. ELNES quantification results (dotted line) for the C–K edge of the (a,b) a-C:H and (c,d) ta-C from regions of different thicknesses t/λ as a function of the lower boundary of the σ^* energy window, superimposed on the corresponding sampled spectrum (solid line) and the reference HOPG spectrum (dash-dotted line). (A color version of this figure can be viewed online.)

3.2. Discussion

In the following we discuss the integration window settings for I_{π^*} and I_{σ^*} . The I_{σ^*} integration window is in general less sensitive for the sp^2 -quantification than that of the I_{π^*} window. We have tested the positions of the two boundaries of the I_{σ^*} window by varying one of them separately with the other fixed to show the direct influence on the $sp^2\%$ quantification. As to the variation of the upper boundary of the I_{σ^*} window, the first non-stable range (sector I) can be attributed to the too small size of the I_{σ^*} integration range to average the pronounced ELNES of crystalline HOPG which is used as a reference for the sp^2 -determination in Equation (3). In the third range (sector III), the first general concern would be the plural scattering or error in the corresponding plural scattering removal. Taking the a-C:H spectra as an example (cf. Fig. 3(a,b)) in context with the low-loss spectra (Fig. 2), multiple scattering by the σ plasmon excitation could contribute to the C–K edge signal in a range starting ~ 16.5 eV above its threshold and reaching a maximum at ~ 23 eV, i.e., such contributions should be increasingly noticeable from ~ 301 eV to ~ 307 eV (considering the onset of C–K edge at 284 eV). A stable range (sector II) with nearly constant $sp^2\%$ shows up between 300 eV and 314 eV for the a-C:H specimen indicating a minor influence of the plural scattering removal process. For the ta-C specimen, multiple scattering contributions to the C–K edge should energetically shifted to higher energy losses according to the low-loss spectra and contribution to the C–K edge should start to be noticeable from ~ 303 to ~ 305 eV and reach a maximum at ~ 311 – 313 eV. In contrast to a-C:H, the range with stable $sp^2\%$ extends from 297 eV to 307 eV for the ta-C specimen,

which largely avoids the region that may contain plural scattering contributions. Although a precise understanding of the behavior of the evaluated $sp^2\%$ in this energy loss range is still lacking, it is clear that the stable ranges all give standard deviations smaller than 0.01 for both spectra of each sample. This indicates that the fine structure of crystalline HOPG is better averaged, and errors in plural scattering removal as well as differences of the ELNES between the two DLC materials and reference spectra are small within this energy loss range.

We did not consider the contributions of π plasmon excitation to the C–K edge, which is less of a problem due to its low intensity compared to that of the σ plasmon. If there was any contribution it would slightly increase the signal in the region of the σ^* peak, owing to the π plasmon energy of 5–6 eV.

With the upper boundary of I_{σ^*} fixed at 307 eV, the effect of varying the lower boundary is demonstrated for the four spectra in Fig. 4. The evaluated $sp^2\%$ in sector I increases which indicates that extra signals in the σ^* window, such as the C–H excitations and the broadening/tail of the π^* excitations between the π^* and σ^* excitations is pronounced, which could cause an underestimation of $sp^2\%$. And, consequently, a slightly increased sp^2 -quantification result as the lower boundary of the σ^* window is moved to higher-energy positions. On the other hand, if the σ^* energy window starts above 298 eV (sector III), the resulting window size could be too small to average the fine structures and, in addition, too sensitive towards errors in plural scattering removal, thus yielding a high standard deviation. The stable region (sector II) with energy windows starting between 292 eV and 300 eV for a-C:H and between 291 eV and 298 eV for ta-C with a standard deviation of less than

0.01, indicates a reasonable integration window.

After all, for the setting of the I_{σ^*} window we found constant $sp^2\%$ with lower boundaries at 292–300 eV (for a-C:H) and 291–298 eV (for ta-C). Regarding the upper boundary, in a good approximation constant sp^2 -values are found for 300–314 eV (for a-C:H) and 297–307 eV (for ta-C) for different specimens with different thicknesses. It is therefore reasonable to routinely fix the σ^* integration window at energy losses between 292 eV and 307 eV. Moreover, the standard deviation of the quantification results can be utilized to gain some knowledge of reliability.

Most critical is the setting of the I_{π^*} integration window. First, the core hole lifetime broadening (0.06 eV) [26] is negligible compared to the energy resolution (0.6–0.7 eV) and can therefore be neglected. Second, different FWHMs of the π^* pre-peaks for the a-C (~2.5 eV) and the HOPG (~1.5 eV) are observed, which can be partially attributed to different life-time broadening effects of the excited states for amorphous and crystalline materials and partially to different densities of states in the considered materials. The FWHM of the π^* pre-peaks is not substantially larger than the energy resolution of ~0.6 eV and a compromise must be made with respect to the choice of energy window which ideally should be significantly larger than the energy resolution. We studied the influence of using a relatively small π^* window on the evaluated $sp^2\%$. The I_{π^*} was always centered on the maximum intensity of the π^* pre-peak. The width of I_{π^*} was initially set to 0.7 eV, close to or slightly larger than the energy resolution. Each boundary of the initial window was varied by ± 0.2 eV, comprising a 0.4-eV-interval slightly more than half of the energy resolution (0.3–0.35 eV), to check the standard deviation of the quantification results. This is a measure of the effectiveness of the compromise we have made and also a measure of the accuracy limited by the energy resolution. The results show that the standard deviation for the quantified $sp^2\%$ is 0.019–0.020 for the a-C:H sample, and 0.009 (thick film region) and 0.015 (thin) for the ta-C sample. The larger standard deviation for the material with higher $sp^2\%$ is in accordance with the larger FWHM of the π^* pre-peak for the a-C:H sample.

It will be demonstrated in Section 4, that the influence of FIB-induced damage for a-C:H specimen is negligible. Hence, by ignoring the local structural variation of the specimen, the standard deviation from the results of 351 sp^2 -quantifications (27 settings of energy windows for 13 C–K spectra) amounts to $\pm 1.7\%$ which indicates the relative accuracy and reliability of the procedure. The comparably narrow π^* integration window largely excludes signals from C–H bonds, distorted C–C bonds and dangling C-bonds [6,8,13,14,18–21], which explains the small standard deviation of the quantification results. The magic angle condition, which could be another source of error, will be discussed in Section 4. It is finally noted that the specific width and position of the energy integration windows for I_{π^*} and I_{σ^*} will depend on the acquisition conditions (electron energy, convergence and acceptance semi-angles). However, our optimization strategy can be generally applied.

With respect to quantification errors, we note that slight shifts and additional features of the π^* and/or σ^* signals can occur in C–K spectra. For example, a shift of the π^* peak by 0.4 eV was observed by Kulik et al. [34] for one sample in a specimen series. The quantification results would be affected by the shift, and a corresponding shift of the energy window would be necessary due to the limited energy resolution (0.6 eV) and the small π^* energy window. Apart from that, the error will mainly be related to the different lifetime broadening of the aC-materials and the HOPG reference. The absolute quantification error is difficult to estimate. It can be determined if reliable sp^2 -quantification data from other techniques are available.

4. Correction of FIB-induced damage from TEM specimen preparation

4.1. Model

STEM/ELNES locally probes the electronic structure and chemical bonding configuration of the material under investigation, and any damage occurring already during sample preparation or later under electron bombardment will directly affect the obtained results. For carbon materials, such effects are of importance if ELNES features are used to quantify the $sp^2\%$. In this section we will present results on the influence of FIB-based TEM specimen preparation. This is a preferable technique for cross-sectional TEM specimen because it allows a site-selective cross-section view of the layer structure. It is also well suited for the preparation of TEM samples containing materials with different Ar⁺-ion sputtering rates (in our case DLC on steel substrates). Moreover, large pieces of the magnetic steel substrates in conventionally prepared TEM specimens would seriously hamper TEM studies. Unfortunately, high-energy Ga⁺-ions may damage the original structure at the milled surfaces of the TEM cross-section specimen. This may even apply if the energy of the Ga⁺-ion is reduced to only a few keV during the final polishing stage. Damaged cover layers of amorphous carbon with modified bonding configurations compared to DLC regions in the interior of the TEM specimen can be generated, leading to errors in quantitative ELNES measurements of the $sp^2\%$.

The model presented in the following is based on the intuitive assumption that the measured $sp^2\%$ depends on the fraction of the damaged layer with respect to the total TEM specimen thickness. It will be tested and applied to DLC and HOPG.

The I -ratio or $sp^2\%$ derived from a C–K edge spectrum is representative for the bond configuration throughout the whole material column defined by the illuminated sample region and can be considered as a linear combination of the bulk contribution and those of the damaged layers on both sides. It is demonstrated by Fig. 5(a) that a damage layer with constant thickness will influence the evaluated $sp^2\%$ depending on the overall TEM sample thickness. The evaluated I -ratio can be written as

$$R = R_b + (R_d - R_b) \cdot T_d \cdot \left(\frac{1}{T}\right) \quad (4)$$

where R denotes the I -ratio for HOPG or $sp^2\%$ for DLCs, and T indicates the total thickness or t/λ of the specimen. Subscripts d and b for R and T represent the damaged and bulk regions in the material column. Ignoring local variations of the properties and consequently assuming T_d , R_d and R_b to be constant, a linear relationship between R and $(1/T)$ can be postulated and the intercept corresponds to R_b . Collecting spectra at different sample thicknesses T then allows to extract R_b .

4.2. Results

Fig. 6 shows C–K edge spectra from three different HOPG specimens after removal of plural scattering. In detail, spectra labeled (1) and (2) were recorded from HOPG specimens of similar orientation, but obtained by different TEM sample preparation techniques, namely scotch-tape cleavage and FIB-preparation. Spectra (2) and (3) were collected from two FIB-prepared TEM specimens, one prepared perpendicular and the other parallel to the graphite basal planes. Each spectrum exhibits more or less pronounced characteristic features of the C–K ELNES as known from graphite: a pronounced π^* pre-peak and a σ^* peak with a maximum at ~292 eV, followed by several oscillations being indicative of the crystalline graphite structure. The three spectra

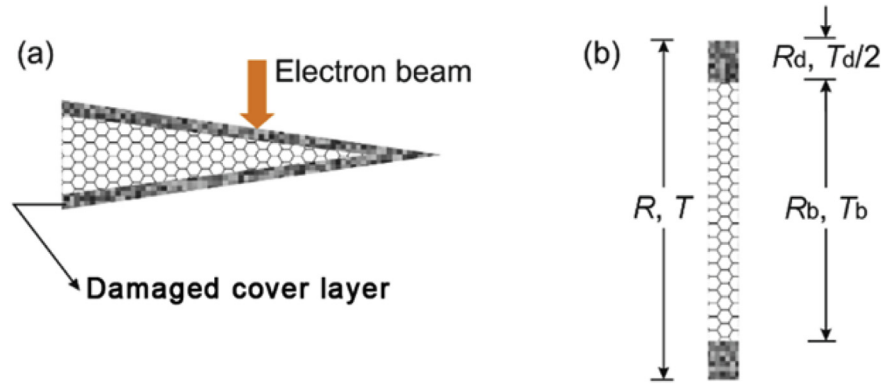


Fig. 5. (a) Scheme of a TEM specimen with damaged surface regions and changing ratio between damaged and undamaged material as a function of the overall sample thickness; (b) material column interacting with the electron beam (overall bond configuration R and overall thickness T , measured by EELS), which is composed of damaged layers on both sides (bond configuration R_d and thickness T_d) and the bulk material (bond configuration R_b and thickness T_b). (A color version of this figure can be viewed online.)

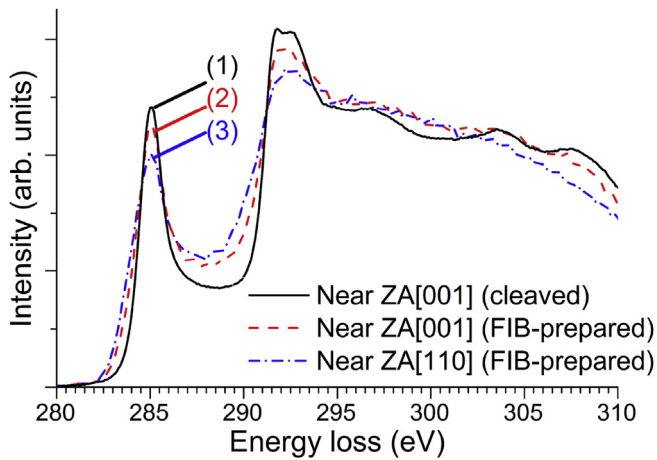


Fig. 6. C–K edge spectra taken under magic-angle conditions from HOPG specimens prepared by (1) scotch tape cleavage, (2) FIB milling parallel to the graphite basal layers, and (3) FIB milling perpendicular to the graphite basal layers. (A color version of this figure can be viewed online.)

were normalized with respect to their integral intensities between 292 and 307 eV. The maximum intensities of the π^* pre-peaks from spectra (1) to (3) show a slight reduction, accompanied by peak broadening.

With the optimized integration window settings, the I_{π^*}/I_{σ^*} intensity ratios of spectra (1)–(3) in Fig. 6 are summarized in Table 1. The relative thicknesses (t/λ) derived from their corresponding low-loss spectra (not shown) are also given. A relatively large range of relative thicknesses t/λ is covered from 0.35 for cleaved HOPG to 0.98 for the FIB-prepared HOPG oriented along the [110] zone axis. Table 1 shows that the ratios I_{π^*}/I_{σ^*} of spectra (2) and (3) are 15% and 8% smaller than that of spectrum (1), which was recorded from cleaved HOPG near to the [001] zone axis.

Quantification of the $sp^2\%$ was performed for all spectra of the a-

Table 1

I_{π^*}/I_{σ^*} ratios derived from the C–K ELNES spectra in Fig. 6 and corresponding relative thicknesses (t/λ) derived from low-loss spectra.

Specimen	$R (I_{\pi^*}/I_{\sigma^*})$	t/λ (relative thickness)
(1) Near [001] ZA (cleaved)	0.046	0.35
(2) Near [001] ZA (FIB-prepared)	0.039	0.58
(3) Near [110] ZA (FIB-prepared)	0.043	0.98

C:H and ta-C specimens by the two window method using Equation (3) with optimized energy-window settings of 284.7–285.3 eV (π^*) and 292–307 eV (σ^*). As a reference, spectrum (1) recorded from the cleaved HOPG reference sample was used. The thickness effect is demonstrated in Fig. 7, where $sp^2\%$ is plotted as a function of the reciprocal relative thickness $(t/\lambda)^{-1}$. Linear fittings were performed on data groups obtained from the a-C:H and ta-C specimens, respectively.

As already been shown in Section 3, for a-C:H the $sp^2\%$ does not differ for thin and thicker specimen regions. As a result, plotting the quantification results as a function of the reciprocal relative thickness and performing a linear fit, a nearly horizontal line is seen (as illustrated by the dashed line in Fig. 7). The linear fit yields the following function in form of Equation (4)

$$R = (0.746 \pm 0.014) + (0.012 \pm 0.008)/T, \quad (5)$$

indicating that the bulk sp^2 -content of a-C:H is $(74.6 \pm 1.4)\%$.

The data set for the ta-C film shows a larger scatter for $sp^2\%$ from 50.3% to 71.3% with t/λ ranging from 0.44 to 1.42, which is well fitted by a linear relationship (dash-dotted line in Fig. 7). In more detail, the $sp^2\%$ values fit better to the line towards the right end of the scale, i.e. for t/λ below 0.7, while the data points deviate more from the fit line at the other end, i.e., for thicker specimen regions. Here, the linear function (cf. Equation (4)) is

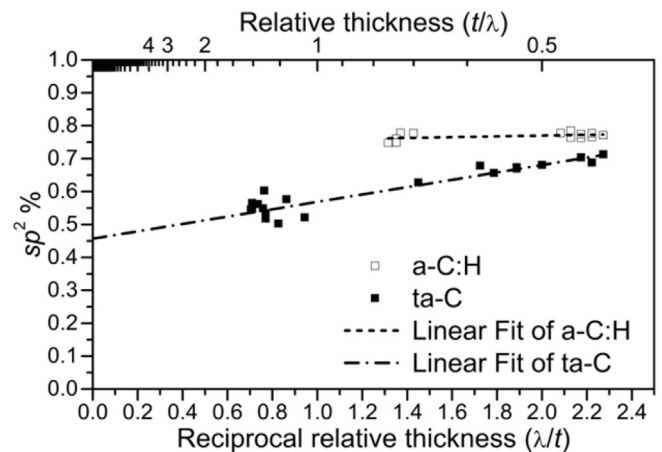


Fig. 7. Quantification of the sp^2 -content by ELNES analyses for the a-C:H and ta-C films as a function of the reciprocal of the relative thickness (λ/t). Dashed/dash-dotted lines are linear fits for each sample.

$$R = (0.457 \pm 0.013) + (0.112 \pm 0.009)/T \quad (6)$$

This suggests that $sp^2\%$ of bulk ta-C is $(45.7 \pm 1.3)\%$.

4.3. Discussion

Spectra (1) and (2) in Fig. 6 were recorded from HOPG specimens with almost the same crystallographic orientation and the anisotropic structure of graphite cannot be responsible for the large difference ($\sim 8\%$) of their I -ratios. Instead, the difference in the I_{π^*}/I_{σ^*} ratio can most likely be attributed to the different sample preparation techniques. The broadened and reduced π^* pre-peak of spectrum (2) implies that the Ga^+ -ion milling could have damaged the surface regions of the TEM specimen where the ordered crystal structure was amorphized. This is also confirmed by HRTEM images of the FIB-prepared HOPG sample in [110] zone axis (not shown), where the lattice fringes are highly disturbed. It can be assumed that C-atoms were transformed from sp^2 -hybridized into sp^3 -hybridized ones or carbon atoms with distorted bonds whereas the crystallinity of graphite is essentially unchanged in the cleaved HOPG specimen. With respect to the difference between spectra (2) and (3), an angular effect due to the orientation difference as large as $\sim 90^\circ$ between them could be considered as reason. Also, this difference could be due to a thickness effect because the fraction of a FIB-induced damaged layer is smaller for a thick specimen and thus the I -ratio is higher, which is the case for spectrum (3) compared to spectrum (2).

By assuming that the FIB-damaged layers are of the same thickness and that the original bond configuration was identical for the specimens corresponding to spectra (2) and (3), Equation (4) was applied and the I -ratio for the undamaged bulk R_b was derived. The I -ratio corrected for the FIB damage well agrees with the I -ratio from spectrum (1), which is free of FIB damage, with a small difference of $\sim 3\%$ compared to the original difference of 8% for spectrum (2) and 15% for spectrum (3). Hence, it can be concluded that the FIB-induced damage is responsible for the different I -ratios of spectra (1)–(3). This also validates our magic angle condition and the model for correcting the influence of the FIB-induced damage.

Using the damage-free spectrum (1) in Fig. 6 as a reference (100% sp^2 -hybridized C-atoms), a linear relationship between $sp^2\%$ and $(t/\lambda)^{-1}$ is obvious for ta-C, showing again good validation of the model. The fitting result yields a corrected $sp^2\%$ of 45.7% with a standard deviation of $\pm 1.3\%$ which is similar to the standard deviation of the ELNES quantification for the a-C:H specimen in Section 3. The corrected sp^2 -content fits well into the typical range of $10\text{--}60\%$ for ta-C in the ternary phase diagram of chemical bonds for the amorphous C–H system [1], noting that the as-measured sp^2 -content ($50\text{--}71\%$) was slightly beyond this range. Several factors could affect the fit quality. First, it is noted that the data from the thick region of the ta-C specimen shows a stronger deviation from the linear fit, possibly due to the error in plural scattering removal for t/λ exceeding 1. Although we have already considered this problem by excluding the plasmon intensity from the σ^* integration window, it is clear that the plasmon intensities extend to a large range of energy loss and is difficult to avoid completely in the energy window. Another factor could be that the low-loss spectrum was not recorded at exactly the same position as the C–K edge spectrum. The low-loss and the C–K edge spectra were recorded separately, and several experimental parameters have to be adjusted due to different acquisition efficiencies. As a result, specimen drift is possible during this process, and the measured thickness for the corresponding $sp^2\%$ could contain an error, leading to a discrepancy for the linear fit. Other factors, such as local structure and thickness fluctuations for the bulk material and the

damaged layer influence the fit as well.

For the a-C:H specimen, the $sp^2\%$ is hardly influenced by the thickness as indicated by the nearly-zero slope of the fit curve, which can be attributed to two possibilities: The specimen does not contain a FIB-damage layer ($T_d = 0$) or the damaged a-C layer contains the same $sp^2\%$ as the bulk ($R_d - R_b = 0$). The first possibility that the Ga^+ -ions could have milled away the material directly without inducing a damaged layer is unlikely, because even for HOPG containing 100% sp^2 -hybridized C-atoms, FIB thinning along the graphite basal planes involves a phase transition as well. Given the small standard deviation (0.011) of the $sp^2\%$ dataset for a-C:H, we can assume that this material contains the same $sp^2\%$ as the FIB-induced amorphous carbon, which is $\sim 75\%$ (see extrapolation of the curve in Fig. 7). Assuming further that $R_d \sim 75\%$ is transferrable to the ta-C specimen, the relative thickness of the damaged layer can be estimated from the slope of the straight line according to Equation (4), which is 0.39, corresponding to a total thickness of ~ 40 nm and a damage depth of ~ 20 nm.

The model for FIB-induced damage correction has a straightforward background. However, a number of assumptions have to be made. The assumption of a damaged layer being homogeneous in both thickness and bond configuration, could be largely valid as seen from studies of FIB-induced damage of Si [35], where the crystal structure of the cross-section of a FIB lamella was studied by TEM. However, this technique is not accessible for the amorphous DLC material with a structure that is undistinguishable from the damaged layer. With respect to the bonding configuration of the damaged layer, to consider it to be transferrable from one amorphous carbon material (the a-C:H film) to another (the ta-C film) for estimating the damaged depth is a postulate and requires further studies.

5. Conclusions

Two different DLC materials, a hydrogenated sp^2 -rich a-C:H film and a ta-C film with lower sp^2 -content, were utilized to test and optimize the quantification procedure for the fraction of sp^2 -hybridized C-atoms based on the ELNES of the C–K ionization edge. The classical two-window method was used to quantify the I_{π^*}/I_{σ^*} intensity ratio and sp^2 -content because of its advantages of ease use and flexible energy-loss signal selection which can be optimized by considering solid state physics aspects. We suggest an optimization strategy which requires the identification of energy-loss integration window ranges with stable quantification results, i.e., with minimum variation of the evaluated sp^2 -content. In practice, the width of the integration windows related to the π^* and σ^* states is optimized by an iterative process by varying only one integration boundary with constant positions of the others. The setting for the π^* states constitutes a compromise between the experimental broadening and lifetime broadening of excited states. We find that a narrow integration window largely excludes contributions from C–H bonds, distorted C-bonds with loss signals between the π^* peak and σ^* loss intensities, as well as that from dangling C-bonds below the π^* peak.

ELNES quantification yields an average sp^2 -content of 76.6% for the a-C:H sample, where a small standard deviation $\pm 1.7\%$ was obtained by statistical analysis. Quantification of the sp^2 -content of the ta-C DLC material gives $(54.3 \pm 1.9)\%$ for thick TEM specimen regions and $(67.2 \pm 1.2)\%$ for thin ones hinting to the damaging influence of FIB-based TEM specimen preparation.

A model for the analysis and correction of the influence of the FIB-induced damage of TEM specimens is suggested. Although several assumptions must be made, such as uniformity of the thickness and bond configuration of the FIB-induced damaged layer, the validity of this method is confirmed by comparing FIB-

prepared and cleaved HOPG TEM specimens. Applying the model for the correction the FIB-induced damage in the ta-C specimen results in a true sp^2 -content of ~46%. This demonstrates that FIB-induced damage cannot be neglected and even more gentle milling conditions need to be applied to minimize damage at TEM sample surfaces.

Acknowledgments

Xinyi Zhang acknowledges funding from China Scholarship Council (CSC) (No. 2010606030). We thank Manuel Mee and Sven Maier (Fraunhofer Institute for Mechanics of Materials, Freiburg, Germany) and Peter Gumbsch (Fraunhofer Institute for Mechanics of Materials, Freiburg, Germany and Institute for Applied Materials, Karlsruhe Institute of Technology, Germany) for providing DLC materials and enlightening discussions.

References

- [1] J. Robertson, Diamond-like amorphous carbon, *Mat. Sci. Eng. R.* 37 (4–6) (2002) 129–281.
- [2] A. Grill, Review of the tribology of diamond-like carbon, *Wear* 168 (1–2) (1993) 143–153.
- [3] J. Vetter, 60 years of DLC coatings: historical highlights and technical review of cathodic arc processes to synthesize various DLC types, and their evolution for industrial applications, *Surf. Coat. Technol.* 257 (2014) 213–240.
- [4] J.T. Titantah, D. Lamoen, sp^3/sp^2 characterization of carbon materials from first-principles calculations: X-ray photoelectron versus high energy electron energy-loss spectroscopy techniques, *Carbon* 43 (6) (2005) 1311–1316.
- [5] A.C. Ferrari, J. Robertson, Raman spectroscopy of amorphous, nanostructured, diamond-like carbon, and nanodiamond, *Philos. Trans. Ser. A Math. Phys. Eng. Sci.* 2004 (362) (1824) 2477–2512.
- [6] P.R. Bressler, M. Lubbe, D.R.T. Zahn, W. Braun, X-ray absorption spectroscopy study of different solid carbon modifications, *J. Vac. Sci. Technol. Vac. Surfaces Films* 15 (4) (1997) 2085–2087.
- [7] R.F. Egerton, Electron energy-loss spectroscopy in the TEM, *Rep. Prog. Phys.* 72 (1) (2009) 016502.
- [8] J. Fink, T. Mullerheinzerling, J. Pfluger, A. Bubenzer, P. Koidl, G. Crecelius, Structure and bonding of hydrocarbon plasma generated carbon-films: an electron-energy loss study, *Solid State Commun.* 47 (9) (1983) 687–691.
- [9] J. Bruley, D.B. Williams, J.J. Cuomo, D.P. Pappas, Quantitative near-edge structure analysis of diamond-like carbon in the electron microscope using a two-window method, *J. Microsc.* 180 (1) (1995) 22–32.
- [10] S.D. Berger, D.R. McKenzie, P.J. Martin, EELS analysis of vacuum arc-deposited diamond-like films, *Philos. Mag. Lett.* 57 (6) (1988) 285–290.
- [11] J.J. Cuomo, J.P. Doyle, J. Bruley, J.C. Liu, Sputter deposition of dense diamond-like carbon films at low temperature, *Appl. Phys. Lett.* 58 (5) (1991) 466–468.
- [12] N. Bernier, F. Bocquet, A. Allouche, W. Saikaly, C. Brosset, J. Thibault, et al., A methodology to optimize the quantification of sp^2 carbon fraction from K edge EELS spectra, *J. Electron Spectrosc. Relat. Phenom.* 164 (1–3) (2008) 34–43.
- [13] S.R.P. Silvaf, J. Robertson, Amaratunga GAJ. Rusli, J. Schwan, Structure and luminescence properties of an amorphous hydrogenated carbon, *Philos. Mag. Part B* 74 (4) (1996) 369–386.
- [14] A. Papworth, C. Kiely, A. Burden, S. Silva, G. Amaratunga, Electron-energy-loss spectroscopy characterization of the sp^2 bonding fraction within carbon thin films, *Phys. Rev. B* 62 (19) (2000) 12628–12631.
- [15] G. Bertoni, J. Verbeeck, Accuracy and precision in model based EELS quantification, *Ultramicroscopy* 108 (8) (2008) 782–790.
- [16] J. Verbeeck, G. Bertoni, Model-based quantification of EELS: is standardless quantification possible? *Microchim. Acta* 161 (3–4) (2008) 439–443.
- [17] J. Titantah, D. Lamoen, Technique for the sp^2/sp^3 characterization of carbon materials: *ab initio* calculation of near-edge structure in electron-energy-loss spectra, *Phys. Rev. B* 70 (7) (2004).
- [18] J.G. Buijnsters, R. Gago, I. Jimenez, M. Camero, F. Agullo-Rueda, C. Gomez-Aleixandre, Hydrogen quantification in hydrogenated amorphous carbon films by infrared, Raman, and X-ray absorption near edge spectroscopies, *J. Appl. Phys.* 105 (9) (2009) 093510.
- [19] D.T.L. Alexander, J.R. Anderson, L. Forró, P.A. Crozier, The real carbon K-edge, *Microsc. Microanal.* 14 (S2) (2008) 674–675.
- [20] D.L. Pappas, K.L. Saenger, J. Bruley, W. Krakow, J.J. Cuomo, T. Gu, et al., Pulsed laser deposition of diamond-like carbon-films, *J. Appl. Phys.* 71 (11) (1992) 5675–5684.
- [21] P. Fallon, V. Veerasamy, C. Davis, J. Robertson, G. Amaratunga, W. Milne, et al., Properties of filtered-ion-beam-deposited diamond like carbon as a function of ion energy, *Phys. Rev. B* 48 (7) (1993) 4777–4782.
- [22] P.E. Batson, Carbon 1s near-edge-absorption fine structure in graphite, *Phys. Rev. B* 48 (4) (1993) 2608–2610.
- [23] N.D. Browning, J. Yuan, L.M. Brown, Real-space determination of anisotropic electronic structure by electron energy loss spectroscopy, *Ultramicroscopy* 38 (3–4) (1991) 291–298.
- [24] D.A. Muller, D.J. Singh, J. Silcox, Connections between the electron-energy-loss spectra, the local electronic structure, and the physical properties of a material: a study of nickel aluminum alloys, *Phys. Rev. B* 57 (14) (1998) 8181–8202.
- [25] C. Hebert, Practical aspects of running the WIEN2k code for electron spectroscopy, *Micron* 38 (1) (2007) 12–28.
- [26] M.O. Krause, Atomic radiative and radiationless yields for K-shells and L-shells, *J. Phys. Chem. Ref. Data* 8 (2) (1979) 307–327.
- [27] P. Moreau, F. Boucher, G. Goglio, D. Foy, V. Mauchamp, G. Ouvrard, Electron energy-loss spectra calculations and experiments as a tool for the identification of a lamellar C_3N_4 compound, *Phys. Rev. B* 73 (19) (2006) 195111.
- [28] R.F. Egerton, P. Li, M. Malac, Radiation damage in the TEM and SEM, *Micron* 35 (6) (2004) 399–409.
- [29] C. Hebert, P. Schattschneider, H. Franco, B. Jouffrey, ELNES at magic angle conditions, *Ultramicroscopy* 106 (11–12) (2006) 1139–1143.
- [30] L. Pastewka, S. Moser, M. Moseler, B. Blug, S. Meier, T. Hollstein, et al., The running-in of amorphous hydrocarbon tribocoatings: a comparison between experiment and molecular dynamics simulations, *Int. J. Mater. Res.* 99 (10) (2008) 1136–1143.
- [31] L.A. Giannuzzi, Introduction to Focused Ion Beams. Instrumentation, Theory, Techniques and Practice, Springer, 2005.
- [32] A.K. Geim, K.S. Novoselov, The rise of graphene, *Nat. Mater* 6 (3) (2007) 183–191.
- [33] J. Kulik, Y. Lifshitz, G.D. Lempert, J.W. Rabalais, D. Marton, Electron-energy-loss spectroscopy of mass-selected ion-beam-deposited diamond-like carbon, *J. Appl. Phys.* 76 (9) (1994) 5063–5069.
- [34] J. Kulik, G.D. Lempert, E. Grossman, D. Marton, J.W. Rabalais, Y. Lifshitz, Sp^3 content of mass-selected ion-beam-deposited carbon films determined by inelastic and elastic electron scattering, *Phys. Rev. B* 52 (22) (1995) 15812–15822.
- [35] N.I. Kato, Y. Kohno, H. Saka, Side-wall damage in a transmission electron microscopy specimen of crystalline Si prepared by focused ion beam etching, *J. Vac. Sci. Technol. Vac. Surfaces Films* 17 (4) (1999) 1201–1204.